JCTC Journal of Chemical Theory and Computation

Activation of H−H, C−H, C−C and C−Cl Bonds by Pd and $PdCl^-$. Understanding Anion Assistance in C−X Bond Activation

Axel Diefenbach,[†] G. Theodoor de Jong,[‡] and F. Matthias Bickelhaupt*[,‡]

Fachbereich Chemie der Philipps-Universität Marburg, Hans-Meerwein-Strasse, D-35032 Marburg, Germany, and Afdeling Theoretische Chemie, Scheikundig Laboratorium der Vrije Universiteit, De Boelelaan 1083, NL-1081 HV Amsterdam, The Netherlands

Received September 2, 2004

Abstract: To understand the mechanism of anion assistance in palladium-catalyzed H−H, C−H, C−C and C−Cl bond activation, several mechanistic pathways for oxidative addition of Pd and $PdCl^-$ to H_2 (H−H), CH_4 (C−H), C_2H_6 (C−C and C−H) and CH_3Cl (C−Cl) were studied uniformly at the ZORA-BP86/TZ(2)P level of relativistic nonlocal density functional theory (DFT). Oxidative addition of the neutral, uncoordinated Pd atom proceeds, as reported earlier, via direct oxidative insertion ($\Delta H^{\ddagger}_{298}$ is −22 to 10 kcal/mol), whereas straight S_N2 substitution (yielding, e.g., $PdCH_3^+ + X^-$) is highly endothermic (144−237 kcal/mol) and thus not competitive. Anion assistance (i.e., going from Pd to $PdCl^-$) lowers all activation barriers and increases the exothermicity of all model reactions studied. The effect is however selective: it favors the highly endothermic S_N2 mechanism over direct oxidative insertion (OxIn). Activation enthalpies $\Delta H^{\ddagger}_{298}$ for oxidative insertion of $PdCl^-$ increase along C−H (−14.0 and −13.5 kcal/mol for CH_4 and C_2H_6) ≈ C−Cl (−11.2 kcal/mol) < C−C (6.4 kcal/mol), i.e., essentially in the same order as for neutral Pd. Interestingly, in case of $PdCl^- + CH_3Cl$, the two-step mechanism of S_N2 substitution followed by leaving-group rearrangement becomes the preferred mechanism for oxidative addition. The highest overall barrier of this pathway (−20.2 kcal/mol) drops below the barrier for direct oxidative insertion (−11.2 kcal/mol). The effect of anion assistance is analyzed using the Activation Strain model in which activation energies $\Delta E^{\ddagger}$ are decomposed into the activation strain $\Delta E^{\ddagger}_{\text{strain}}$ of and the stabilizing transition state (TS) interaction $\Delta E^{\ddagger}_{\text{int}}$ between the reactants in the activated complex: $\Delta E^{\ddagger} = \Delta E^{\ddagger}_{\text{strain}} + \Delta E^{\ddagger}_{\text{int}}$. For each type of activated bond and reaction mechanism, the activation strain $\Delta E^{\ddagger}_{\text{strain}}$ adopts characteristic values which differ only moderately, within a relatively narrow range, between corresponding reactions of Pd and $PdCl^-$. The lowering of activation barriers through anion assistance is caused by the TS interaction $\Delta E^{\ddagger}_{\text{int}}$ becoming more stabilizing.

1. Introduction

Oxidative addition (eq 1) is a key step in many catalytic reactions[1] and has been intensively investigated both experimentally[2−7] and theoretically.[5,7−12]

$$ML_n + R{-}X \underset{\text{Reductive Elimination}}{\overset{\text{Oxidative Addition}}{\rightleftharpoons}} R{-}ML_n{-}X \qquad (1)$$

In the present study, we aim at understanding how anion assistance, i.e., the introduction of an additional, negatively charged ligand, influences a catalyst's electronic structure and how this in turn affects its reactivity toward the archetypical H−H, C−H, C−C and C−Cl bonds in H_2, CH_4,

* Corresponding author fax: +31−20−59 87629; e-mail: FM.Bickelhaupt@few.vu.nl.

[†] Fachbereich Chemie der Philipps-Universität Marburg. Present address: Sercon GmbH.

[‡] Scheikundig Laboratorium der Vrije Universiteit.

10.1021/ct0499478 CCC: $30.25 © 2005 American Chemical Society
Published on Web 02/03/2005

C_2H_6 and CH_3Cl. This is of interest also for industrial chemistry because it enables a more rational design of catalytically active species. One example is the activation and subsequent functionalization of the rather inert alkanes (e.g. CH_4).[13] Thus, a detailed study of the reactivity of $PdCl^-$ toward H_2, CH_4, C_2H_6 and CH_3Cl has been carried out using relativistic nonlocal density functional theory (DFT) at the ZORA-BP86/TZ(2)P level (see Section 2). This approach was shown previously to yield reliable trends in reactivity for oxidative insertion of Pd into C−H, C−C and C−Cl bonds of methane, ethane and chloromethane.[14] The reactivity of the monocoordinated $PdCl^-$ complex is then compared with that of the uncoordinated neutral Pd atom that we studied recently.[12] Thus, all together, the potential energy surfaces (PES) of the following model reactions (eqs 2−6) were explored and compared:

$$\text{H−H activation:}\quad Pd + H_2 \rightarrow H-Pd-H \tag{2a}$$

$$PdCl^- + H_2 \rightarrow H-PdCl-H^- \tag{2b}$$

$$\text{C−H activation:}\quad Pd + CH_4 \rightarrow CH_3-Pd-H \tag{3a}$$

$$PdCl^- + CH_4 \rightarrow CH_3-PdCl-H^- \tag{3b}$$

$$Pd + C_2H_6 \rightarrow CH_3CH_2-Pd-H \tag{4a}$$

$$PdCl^- + C_2H_6 \rightarrow CH_3CH_2-PdCl-H^- \tag{4b}$$

$$\text{C−C activation:}\quad Pd + C_2H_6 \rightarrow CH_3-Pd-CH_3 \tag{5a}$$

$$PdCl^- + C_2H_6 \rightarrow CH_3-PdCl-CH_3^- \tag{5b}$$

$$\text{C−Cl activation:}\quad Pd + CH_3Cl \rightarrow CH_3-Pd-Cl \tag{6a}$$

$$PdCl^- + CH_3Cl \rightarrow CH_3-PdCl-Cl^- \tag{6b}$$

For each of the 10 model reactions of eqs 2−6, the direct oxidative insertion (OxIn) mechanism (eq 7) and an alternative S_N2 type reaction which overall leads also to oxidative addition (eq 8) is studied.

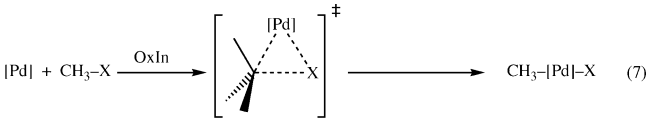

(7)

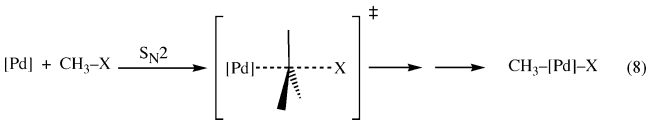

(8)

In this way, one achieves a uniform treatment of different reaction mechanisms for the broad spectrum of H−H, C−H, C−C and C−Cl bond activation induced by Pd and $PdCl^-$.

The effect of anion assistance on the competition between the various bond activation processes and mechanisms is interpreted in terms of the Activation Strain model of chemical reactivity originally introduced in the context of elementary organic reactions.[10,12] In this model, activation energies $\Delta E^{\ddagger}$ are decomposed into the activation strain $\Delta E^{\ddagger}_{\text{strain}}$ of and the stabilizing transition state (TS) interaction $\Delta E^{\ddagger}_{\text{int}}$ between the reactants in the activated complex: $\Delta E^{\ddagger} = \Delta E^{\ddagger}_{\text{strain}} + \Delta E^{\ddagger}_{\text{int}}$. Recently, in our study on oxidative addition of H−H and C−X bonds to uncoordinated Pd, we have shown that the activation strain adopts characteristic values for a particular bond and reaction mechanism. At this point, we anticipate that the activation strain preserves these characteristic values also after introducing a chloride ligand, i.e., on going from Pd to $PdCl^-$. The lowering of activation barriers that results from anion assistance turns out to be caused by the TS interaction $\Delta E^{\ddagger}_{\text{int}}$, which becomes more stabilizing. We show how the concepts of activation strain and TS interaction can be used to rationally tune our model catalyst's stereochemical selectivity toward retention or inversion of configuration of the carbon atom involved in C−X bond activation.

The long-term purpose of these efforts is understanding and directing, in a rational manner, the factors that determine the catalytic activity and selectivity of *solution-phase* transition metal *complexes*. However, as pointed out before, the starting point is the investigation of the *intrinsic* reactivity of the transition metal *atom*.[9,12] Now, by introducing ligands in a second stage, it can be precisely assessed how they interfere with the metal electronic structure and why exactly they cause a particular change in the activity and selectivity of the resulting homogeneous catalyst. This modular approach to theoretical homogeneous catalysis, in which the catalyst is assembled step by step to uncover and understand the function of its individual components, has been designated Fragment-oriented Design of Catalysts (FDC). The present study focuses on introducing a single (but important) ligand and thus marks the beginning of stage 2 that we continue to tackle soon. Eventually, in a third stage, the effect of solvent molecules is explored in an analogous manner.

This paper is organized as follows. After describing our quantum chemical method in Section 2, we proceed in Section 3.1 with the exploration of the PES of the various model reactions. Next, in Section 3.2, the Activation Strain model of chemical reactivity is presented. This model is applied in Section 3.3 in which the effect of anion assistance on the competition between the different model bond activation processes, i.e., the relative heights of activation barriers, is analyzed. The conclusions are summarized in Section 4.

2. Methods

All calculations are based on density functional theory (DFT)[15,16] and have been performed using the Amsterdam Density Functional (ADF) program.[17] MOs were expanded in a large uncontracted set of Slater-type orbitals (STOs).[17h] For H, C and Cl, the basis is of triple-ζ quality, augmented with two sets of polarization functions: 2*p* and 3*d* for hydrogen and 3*d* and 4*f* for carbon and chlorine. The Pd atom is represented by a triple-ζ type basis set augmented with one set of 5*p* polarization functions. The core shells of carbon (1*s*), chlorine (1*s*2*s*2*p*) and palladium (1*s*2*s*2*p*3*s*3*p*3*d*) were treated by the frozen-core approximation.[17b] An auxiliary set of *s*, *p*, *d*, *f* and *g* STOs was used to fit the molecular

Table 1. Reaction Profiles for the Oxidative Insertion (OxIn), S_N2 Substitution and S_N2/Cl-Rearrangement Reactions of Pd (from Ref 12a) and $PdCl^-$ (This Work) with H_2, CH_4, C_2H_6 and CH_3Cl, Respectively: 298 K Enthalpies (in kcal/mol) Relative to Reactants[a]

activated bond	reactants	reactant complex	transition state	product
		Oxidative Insertion		
H−H	Pd + H_2	−24.4 (−24.1[b])	−21.7 (−21.7[b])	−21.1[c] (−22.2[b])
	$PdCl^-$ + H_2	−36.3	[d]	[d]
C−H	Pd + CH_4	−11.4	−5.0	−9.7
	$PdCl^-$ + CH_4	−17.5	−14.0	−15.5
	Pd + C_2H_6	−11.6	−4.1	−11.6[e]
	$PdCl^-$ + C_2H_6	−17.7	−13.5	−16.1[f]
C−C	Pd + C_2H_6	−11.6	9.6	−14.1
	$PdCl^-$ + C_2H_6	−17.7	6.4	−16.0
C−Cl	Pd + CH_3Cl	−15.6	−6.0	−35.7
	$PdCl^-$ + CH_3Cl	−20.7	−11.2	−58.7
		S_N2 Substitution		
H−H	Pd + H_2	−24.4[g]	[h]	237.0[i]
	$PdCl^-$ + H_2	−36.3[g]	[h]	78.5[i]
C−H	Pd + CH_4	−11.4	[h]	228.7[i]
	$PdCl^-$ + CH_4	−17.5	[h]	88.2[i]
C−C	Pd + C_2H_6	−11.6	[h]	228.6[i]
	$PdCl^-$ + C_2H_6	−17.7	[h]	88.1[i]
C−Cl	Pd + CH_3Cl	−10.1	[h]	143.5[i]
	$PdCl^-$ + CH_3Cl	−23.9	−22.8[j]	(−24.1)[k] 3.0 [i]
		S_N2/Cl-Rearrangement		
C−Cl	Pd + CH_3Cl	−10.1	21.2	−35.7
	$PdCl^-$ + CH_3Cl	−23.9	−22.8[j]	(−24.1)[k]
			−20.2[l]	−58.7[m]

[a] Computed at BP86/TZ(2)P (see also Figures 1−6). [b] Electronic energies. [c] No reverse activation enthalpy. [d] No stable product. [e] Primary product (P) of insertion. Rearrangement via second TS (at −11.0 kcal/mol) to more stable conformation (at −12.0 kcal/mol). [f] Primary product (P) of insertion. Rearrangement via second TS (at −15.6 kcal/mol) to more stable conformation (at −16.3 kcal/mol). [g] Linear, $C_{\infty v}$ symmetric Pd−H−H (at −8.8 kcal/mol) or $^-$ClPd−H−H structures (at −12.6 kcal/mol) are second-order saddle points. [h] No reverse activation barrier. [i] Products (P) of straight S_N2 substitution. [j] TS of straight S_N2 substitution. [k] Product complex (PC) of straight S_N2 substitution. [l] TS of leaving-group rearrangement, proceeding from PC of straight S_N2 reaction of $PdCl^-$ + CH_3Cl (see footnote i). [m] Oxidative addition product.

density and to represent the Coulomb and exchange potentials accurately in each SCF cycle.[17i]

Geometries and energies were calculated using the generalized gradient approximation (GGA). Exchange is described by Slater's Xα potential,[17j] with nonlocal corrections owing to Becke.[17k,l] Correlation is treated in the Vosko-Wilk-Nusair (VWN) parametrization using formula V,[17m] with nonlocal corrections due to Perdew.[17n] Relativistic effects were taken into account by the zeroth-order regular approximation (ZORA).[18] Prior investigations showed that relativistic effects are significant for our systems and that the ZORA formalism is well suited for describing them.[14]

All energy minima and transition state[17q] structures were verified by frequency calculations:[17r] for minima all normal modes have real frequencies, whereas transition states have one normal mode with an imaginary frequency. The character of the normal mode associated with the imaginary frequency was analyzed to ensure that the correct transition state was found.

Bond enthalpies at 298.15 K and 1 atm (ΔH_{298}) were calculated from electronic bond energies (ΔE) according to eq 9, assuming an ideal gas.[19]

$$\Delta H_{298} = \Delta E + \Delta E_{\mathrm{trans},298} + \Delta E_{\mathrm{rot},298} + \Delta E_{\mathrm{vib},0} + \Delta(\Delta E_{\mathrm{vib},0})_{298} + \Delta(pV) \quad (9)$$

Here, $\Delta E_{\mathrm{trans},298}$, $\Delta E_{\mathrm{rot},298}$ and $\Delta E_{\mathrm{vib},0}$ are the differences between products and reactants in translational, rotational and zero point vibrational energy, respectively; $\Delta(\Delta E_{\mathrm{vib}})_{298}$ is the change in the vibrational energy difference as one goes from 0 to 298.15 K. The vibrational energy corrections are based on the frequency calculations. The molar work term $\Delta(pV)$ is $(\Delta n)RT$; $\Delta n = -1$ for two reactants (e.g. $PdCl^-$ and CH_3X) combining to one species. Thermal corrections for the electronic energy are neglected.

3. Results and Discussion

3.1. Reaction Profiles and Geometries. In this section, we discuss the potential energy surfaces (PES) of the various oxidative insertion and S_N2 reactions as well as the geometries of the transition states of the various reactions. The results are summarized in Figures 1−6 (geometries) and Tables 1−3 (thermochemistry and geometries) and 4 (Activation Strain analyses).

Here, we focus on the reactions of the anionic, monocoordinated $PdCl^-$ and how these differ from the reactions of the neutral, uncoordinated Pd atom. For a full account of the neutral reactions, the reader is referred to ref 12a.

Direct Oxidative Insertion (OxIn). First, the direct oxidative insertion (OxIn) reactions are examined. For both, Pd and $PdCl^-$, and for all substrates, they proceed from a reactant complex via a TS to a product, see Figures 1−5. The effect of anion assistance, i.e., going from Pd to $PdCl^-$, is a substantial stabilization relative to the separate reactants of all stationary points along the PES (see Table 1): reactant

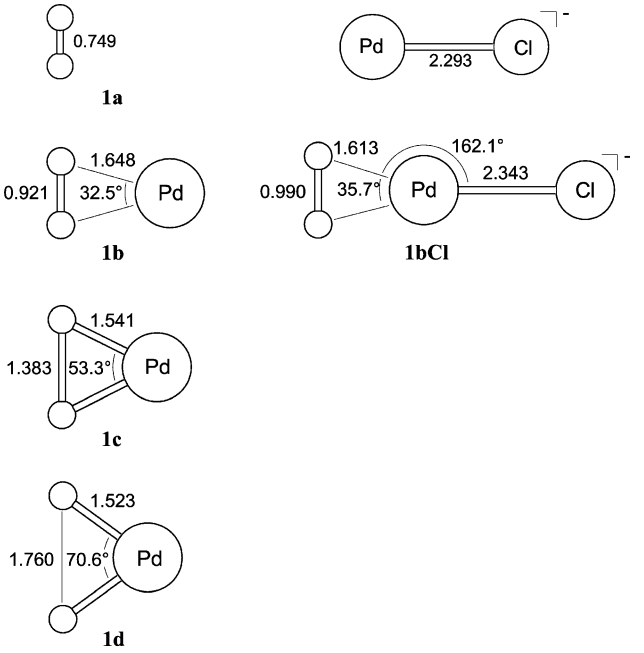

Figure 1. Geometries (in Å, deg) at ZORA-BP86/TZ(2)P of stationary points along the potential energy surface for oxidative insertion (OxIn) reaction of Pd (from ref 12a) and $PdCl^-$ (this work) into the H−H bond of H_2.

complexes gain an additional stabilization of 5−12 kcal/mol, reaction barriers are lowered by 3−14 kcal/mol, and the reactions become overall 2−23 kcal/mol more exothermic. Whereas the oxidative insertion of the uncoordinated Pd + H_2 occurs with a minimal reverse activation energy of only half a kcal/mol, the reverse barrier vanishes completely for the oxidative insertion of $PdCl^- + H_2$, see Table 1. In other words, there is no stable product and the only stationary point left is that of the reactant complex **1bCl** at −36.3 kcal/mol (see Table 1 and Figure 1).

The $PdCl^-$ induced C−H activation is investigated using two different substrates, CH_4 (**2a**) and C_2H_6 (**3a**). In this way, we can reveal if, e.g., the activation strain (see Section 3.2) adopts a characteristic value for a particular type of bond (here, the C−H bond) in different substrates. Geometries for both reactions are shown in Figures 2 and 3, structures **2aCl**-**2dCl** and **3aCl**-**3dCl**. Again, one finds relatively stable reactant complexes, **2bCl** and **3bCl**, respectively, in which $PdCl^-$ binds via palladium symmetrically, in an η^2 fashion, to two C−H bonds of the substrate, similar to the situation found for Pd in **2b** and **3b** (see Figures 3 and 4). Note that in fact all substrates but CH_3Cl form reactant complexes that are of about the same thermodynamic stability as the corresponding product of oxidative addition to $PdCl^-$ (or Pd). For $PdCl^- + CH_4$, eq 3b, the activation enthalpy is −14.0 kcal/mol relative to the reactants. In the TS, **2cCl**, the C−H bond has been stretched by 0.479 Å (44%) and amounts to 1.575 Å, somewhat less than in the corresponding neutral TS, **2c**. The C−H activation of $PdCl^- + C_2H_6$, eq 4b, proceeds via a transition state **3cCl** at −13.5 kcal/mol relative to the reactants, to a product **3dCl** at −16.1 kcal/mol. The C−H bond in TS **3cCl** is lengthened by 0.561 Å (51%) and amounts to 1.660 Å (see Table 2 in which, for the convenience of the reader, we have collected the data on

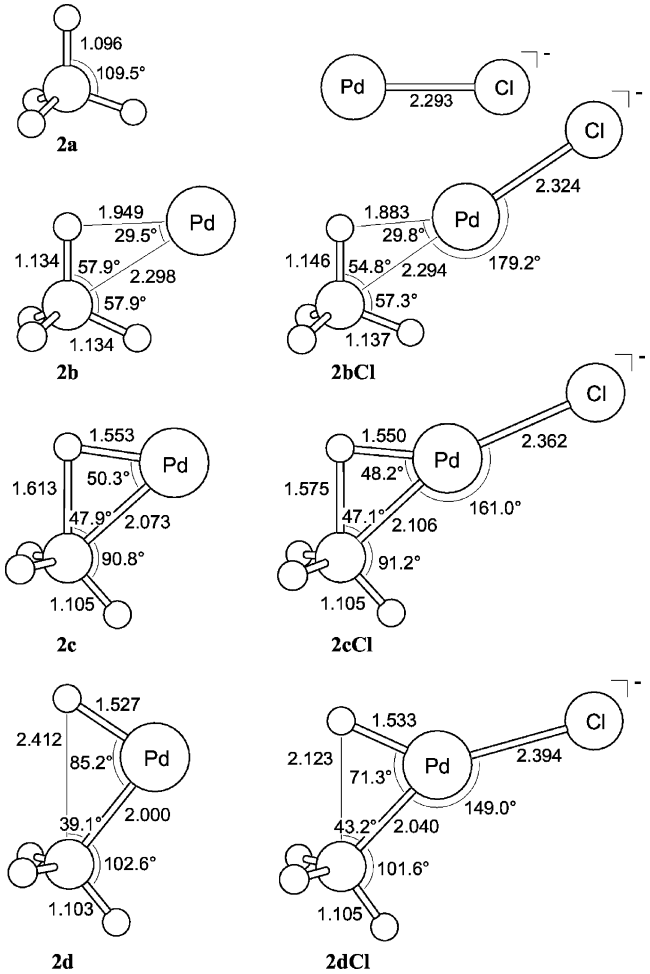

Figure 2. Geometries (in Å, deg) at ZORA-BP86/TZ(2)P of stationary points along the potential energy surface for oxidative insertion (OxIn) reaction of Pd (from ref 12a) and $PdCl^-$ (this work) into the C−H bond of CH_4.

C−X and H−H bond lengths and stretching in the TS). This is very similar to the C−H activation of $PdCl^- + CH_4$. The reaction may further proceed via a second transition state (0.5 kcal/mol above **3dCl** and corresponding to an internal rotation around the Pd−C bond) to a conformation that is 0.2 kcal/mol more stable than the initial product complex **3dCl**.

The OxIn activation of the C−C bond of ethane by $PdCl^-$ (eq 2d) starts from the reactant complex **4bCl**, which is identical to the reactant complex **3bCl** for C−H activation in the same substrate. The barrier associated with the transition state, **4cCl**, is with 6.4 kcal/mol significantly higher than in case of C−H activation. Yet, in this TS, the C−C bond is only stretched by 0.362 Å (24%) and amounts to 1.894 Å; the relative stretching is less than in the case of C−H activation.

The activation of CH_3Cl **5a** by direct oxidative insertion of $PdCl^-$ is connected with a slight lengthening of the C−Cl bond by 0.240 Å (13%) in the TS, where this bond has a length of 2.043 Å. The activation barrier of −11.2 kcal/mol is lower than for C−H and C−C activation. It is also lower than the barrier of −6.0 kcal/mol associated with activation of the same bond by direct oxidative insertion of uncoordinated Pd. The formation of product **5dCl** is the most

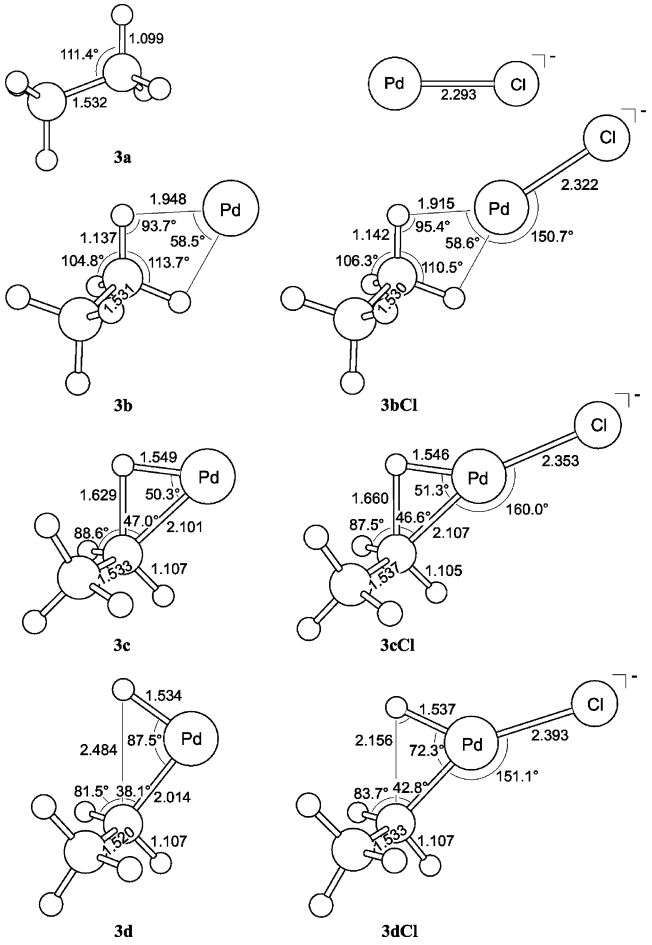

Figure 3. Geometries (in Å, deg) at ZORA-BP86/TZ(2)P of stationary points along the potential energy surface for oxidative insertion (OxIn) reaction of Pd (from ref 12a) and $PdCl^-$ (this work) into the C−H bond of C_2H_6.

exothermic oxidative addition among the model reactions studied, with a reaction enthalpy of −58.7 kcal/mol.

Thus, the 298 K activation enthalpies (relative to the separate reactants) of the anion-assisted reactions increase more or less in the same order as those induced by the bare Pd atom, namely, in the order C−H (−14.0 and −13.5 kcal/mol for CH_4 and C_2H_6) ≈ C−Cl (−11.2 kcal/mol) < C−C (6.4 kcal/mol).[20] (As pointed out above, for $PdCl^-$ + H−H, there is no stable product and thus no TS for oxidative insertion.) The higher barrier for C−C than for C−H activation by uncoordinated Pd originates from a much less favorable TS interaction[12a] with the model catalyst in the former bond and not, as thought previously,[11i,n] from a higher strain associated with the tilting of two methyl groups for C−C activation versus only one methyl group for C−H activation. As will become clear through the Activation Strain analysis in Section 3.3, the same holds true for the present $PdCl^-$ induced C−C and C−H activation processes.

S_N2 Substitution versus Direct Oxidative Insertion. Next, we discuss the S_N2-type reactions and how they compete with direct oxidative insertion. For both, Pd and $PdCl^-$, and for all substrates but CH_3Cl, the actual substitution process of the straight S_N2 reaction, i.e., formation of the new Pd−C (or Pd−H) bond and breaking of the old C−X (or H−H) bond, proceeds from the same reactant complexes

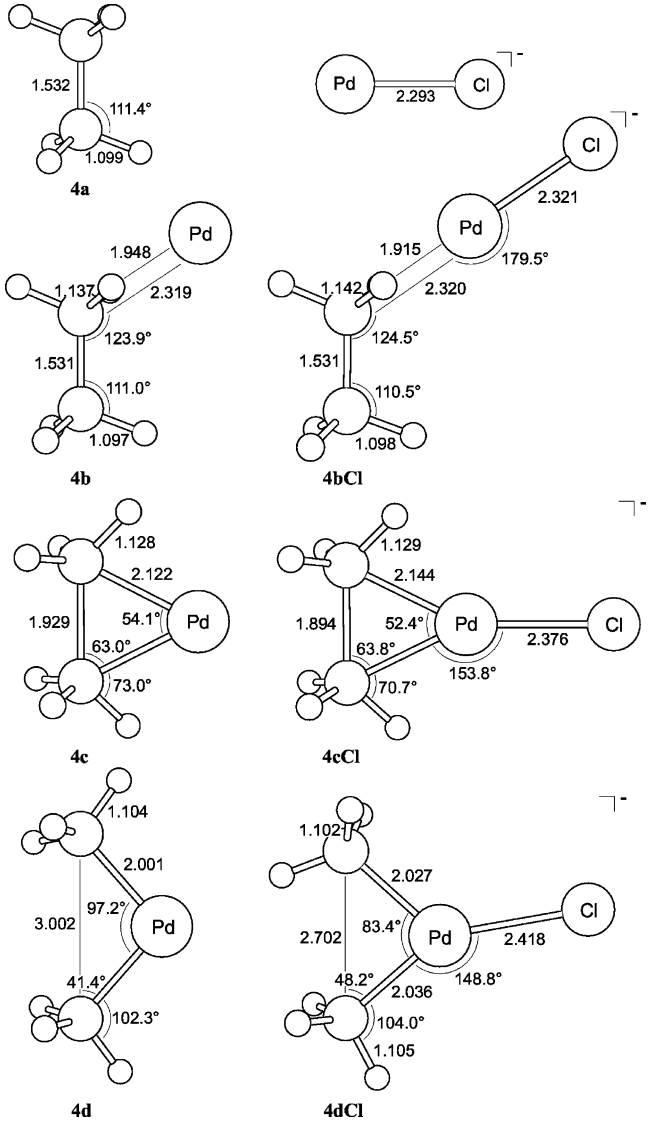

Figure 4. Geometries (in Å, deg) at ZORA-BP86/TZ(2)P of stationary points along the potential energy surface for oxidative insertion (OxIn) reaction of Pd (from ref 12a) and $PdCl^-$ (this work) into the C−C bond of C_2H_6.

as the competing direct oxidative insertion (OxIn) reactions discussed above (see Figures 1−5). The effect of introducing a chloride ligand on palladium, i.e., going from Pd to $PdCl^-$, is a dramatic reduction, by 140 kcal/mol or more, of the endothermicity of the straight S_N2 reaction (see Table 1). The reason for this is that the energetically highly unfavorable charge separation, which occurs in the products of Pd (e.g., $PdCH_3^+ + X^-$), disappears in those of $PdCl^-$ (e.g., $PdClCH_3 + X^-$). Still, in all cases except for the reaction of $PdCl^- + CH_3Cl$, the straight S_N2 reactions are highly endothermic (79−88 kcal/mol) and proceed without a reverse barrier, i.e., without a regular S_N2 transition state. In other words, C−H and C−C bond activation occurs through direct oxidative insertion (OxIn) for both model catalysts, Pd and $PdCl^-$.

The situation is strikingly different for C−Cl activation. For $PdCl^- + CH_3Cl$, a regular S_N2 transition state **6cCl** was found, at −22.8 kcal/mol relative to the reactants, that separates the reactant complex **6bCl** (at −23.9 kcal/mol)

Table 2. Length and Stretching in the TS of the Activated Bond for Direct Oxidative Insertion (OxIn)[a]

activated bond	reactants	length in substr (Å)	length in TS (in Å)		stretching in TS (in Å)		stretching in TS (in %)	
			Pd	$PdCl^-$	Pd	$PdCl^-$	Pd	$PdCl^-$
H−H	$Pd + H_2$	0.749	1.383	[b]	0.634	[b]	85	[b]
C−H	$Pd + CH_4$	1.096	1.613	1.575	0.517	0.479	47	44
	$Pd + C_2H_6$	1.099	1.629	1.660	0.530	0.561	48	51
C−C	$Pd + C_2H_6$	1.532	1.929	1.894	0.397	0.362	26	24
C−Cl	$Pd + CH_3Cl$	1.803	1.968	2.043	0.165	0.240	9	13

[a] Computed at ZORA-BP86/TZ(2)P. [b] No stable product.

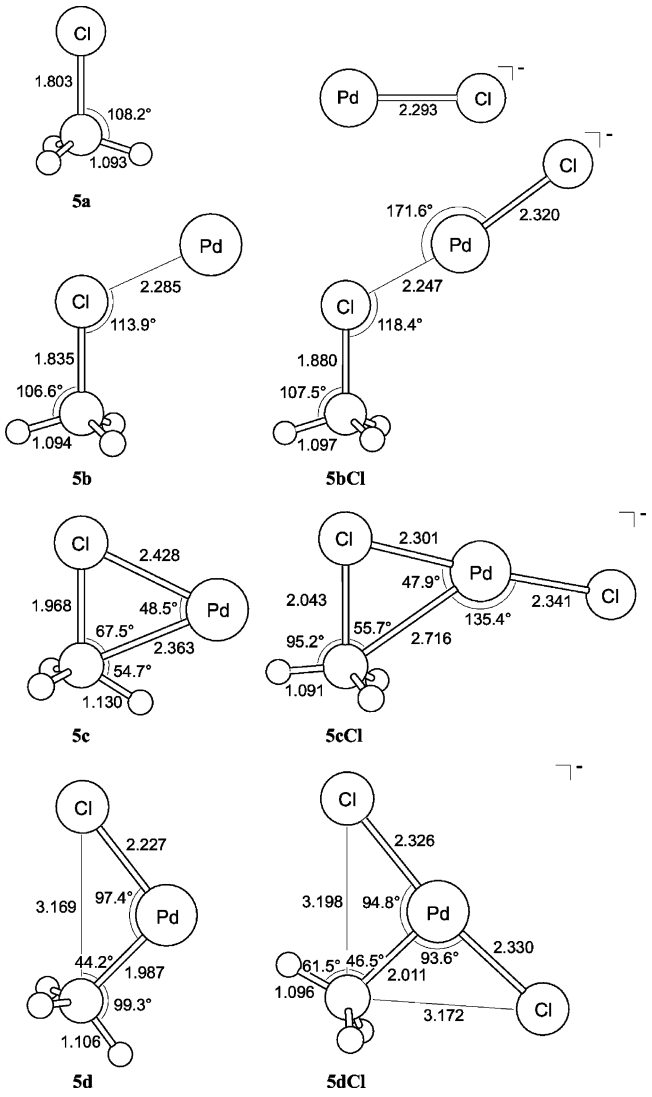

Figure 5. Geometries (in Å, deg) at ZORA-BP86/TZ(2)P of stationary points along the potential energy surface for oxidative insertion (OxIn) reaction of Pd (from ref 12a) and $PdCl^-$ (this work) into the C−Cl bond of CH_3Cl.

from an S_N2 product complex **6dCl** (at −24.1 kcal/mol), see Figure 6. Dissociation of this complex leads to the products of the straight S_N2 substitution at 3.0 kcal/mol relative to reactants (Table 1). In addition, a second transition state **6eCl** was found at −20.2 kcal/mol, which is reached from **6dCl** and corresponds to a rearrangement of the leaving group Cl^- (Cl-ra) yielding the net oxidative addition product **6fCl** at an energy of −58.7 kcal/mol. This product is identical to structure **5dCl** resulting from direct insertion. We recall that for $Pd + CH_3Cl$ a similar pathway (S_N2/Cl-ra) was found which, however, proceeds in one elementary reaction step.[12] This pathway involves a transition state **6e**, 21.2 kcal/mol above the reactants, which has already proceeded beyond the actual substitution stage and has mainly the character of Cl^- rearrangement. Thus, the effect of anion assistance is a lowering of the overall barrier of the S_N2 pathway by 42.4 kcal/mol (from 21.2 kcal/mol in case of **6e** to −20.2 kcal/mol in case of **6eCl**).[21] For the other substrates, a TS associated with an S_N2/Cl-ra mechanism could not be found.

Interestingly, through anion assistance, we have achieved a switch of mechanistic pathway for C−Cl bond activation. While for $Pd + CH_3Cl$ the overall barrier for the pathway of S_N2 substitution followed by Cl^- rearrangement (21.2 kcal/mol) is much higher than that for oxidative insertion (−6.0 kcal/mol), it drops in case of $PdCl^- + CH_3Cl$ to −20.2 kcal/mol, i.e., well below the oxidative insertion barrier of −11.2 kcal/mol. Hence, oxidative addition of the C−Cl bond proceeds through direct oxidative insertion for Pd and through the S_N2 pathway for $PdCl^- + CH_3Cl$. The OxIn mechanism is associated with retention of configuration at the carbon atom of the activated C−X bond, whereas the S_N2/Cl-ra mechanism goes with inversion of configuration. For the present, rather simple model substrate, CH_3Cl, this leads to identical products. However, the two pathways yield different enantiomers as product in case of more complex substrates that involve an asymmetric carbon atom in the activated C−X bond. Thus, by switching anion assistance on or off, we can steer the stereochemical course of the bond activation process. In Section 3.3, we discuss why anion assistance has the effect of shifting the preference from OxIn to S_N2 pathway.

Entropy Effects on Barriers. Entropy effects at 298 K are important in the sense that they increase the magnitude of the activation free energy $\Delta G^{\ddagger}$ by a few kcal/mol, but, as can be seen in Table 3, they do not discriminate much between the various bond activation reactions and pathways considered.

The 298 K activation entropies $\Delta S^{\ddagger}$ for direct oxidative insertion (OxIn) of $PdCl^-$ are somewhat more negative than those of Pd and amount to −29.8 (C−H in methane), −32.2 (C−H in ethane), −32.6 (C−C) and −30.6 cal/mol K (C−Cl). Likewise, the activation entropies for the two steps of the S_N2 pathway to C−Cl bond activation of $PdCl^-$ are more negative than that of the corresponding one-step mechanism of Pd and amount to −31.6 (S_N2 step) and −29.8 cal/mol K (Cl rearrangement). This translates into $-T\Delta S^{\ddagger}$ values of 8.9−9.7 kcal/mol for the reactions involving $PdCl^-$ and 5.4−

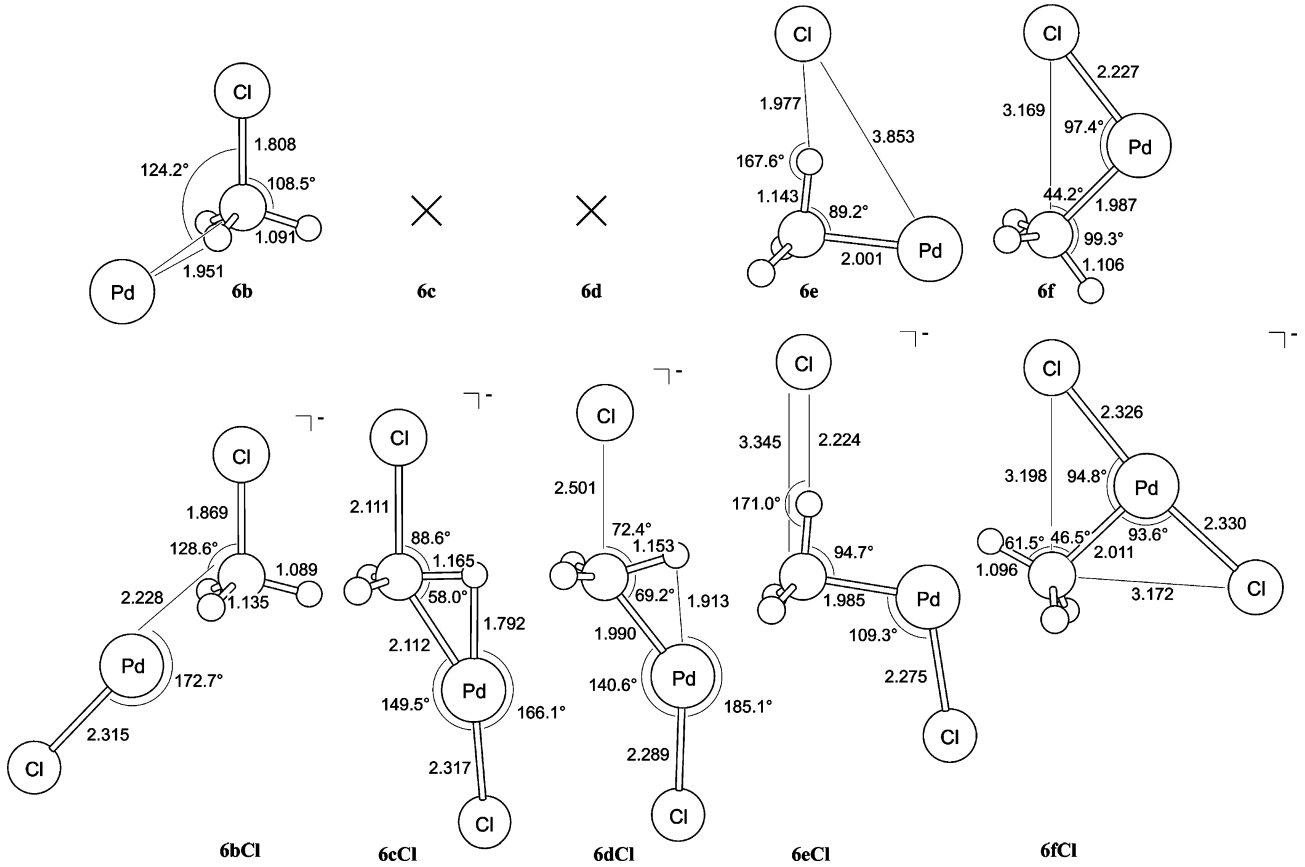

Figure 6. Geometries (in Å, deg) at ZORA-BP86/TZ(2)P of stationary points along the potential energy surface for the S_N2/Cl^--rearrangement reaction of Pd (from ref 12a) and $PdCl^-$ (this work) with CH_3Cl.

Table 3. Entropy Effects at 298 K on Activation Barriers (Relative to Reactants) for the Oxidative Insertion (OxIn) and S_N2/Cl-Rearrangement Reactions of Pd and $PdCl^-$ with H_2, CH_4, C_2H_6 and CH_3Cl, Respectively[a]

activated bond	reactants	$\Delta H^{\ddagger}$	$\Delta S^{\ddagger a}$	$-T\Delta S^{\ddagger a}$	$\Delta G^{\ddagger a}$
	Oxidative Insertion				
H−H	$Pd + H_2$	−21.7	−18.1	5.4	−16.3
	$PdCl^- + H_2$	[b]	[b]	[b]	[b]
C−H	$Pd + CH_4$	−5.0	−22.5	6.7	1.7
	$PdCl^- + CH_4$	−14.0	−29.8	8.9	−5.1
	$Pd + C_2H_6$	−4.1	−24.3	7.3	3.2
	$PdCl^- + C_2H_6$	−13.5	−32.2	9.6	−3.9
C−C	$Pd + C_2H_6$	9.6	−26.1	7.8	17.4
	$PdCl^- + C_2H_6$	6.4	−32.6	9.7	16.1
C−Cl	$Pd + CH_3Cl$	−6.0	−23.4	7.0	1.0
	$PdCl^- + CH_3Cl$	−11.2	−30.6	9.1	−2.1
	S_N2/Cl-Rearrangement				
C−Cl	$Pd + CH_3Cl$	21.2[c]	−21.6[c]	6.5[c]	27.7[c]
	$PdCl^- + CH_3Cl$	−22.8[d]	−31.6[d]	9.4[d]	−13.4[d]
		−20.2[e]	−29.8[e]	8.9[e]	−11.3[e]

[a] Computed at BP86/TZ(2)P (see also Table 1). [b] No stable product. [c] Concerted S_N2/Cl-rearrangement. [d] Separate S_N2 substitution. [e] Separate Cl-rearrangement.

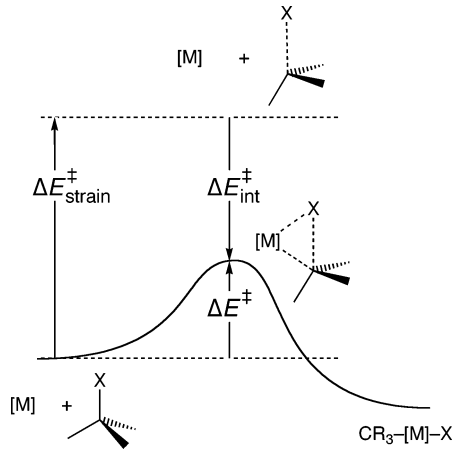

Figure 7. Illustration of the Activation Strain model in case of C−X bond activation by a transition metal system [M]. The activation energy $\Delta E^{\ddagger}$ is decomposed into the activation strain $\Delta E^{\ddagger}_{strain}$ of and the stabilizing TS interaction $\Delta E^{\ddagger}_{int}$ between the reactants in the transition state.

7.8 kcal/mol for those involving Pd. Thus, in terms of relative activation free energies $\Delta G^{\ddagger}$, this does essentially not change the picture that emerges from the relative heights of activation energies $\Delta E^{\ddagger}$ of the various reactions. Therefore, in the following, we focus on further analyzing the origin of and difference between the energy barriers $\Delta E^{\ddagger}$ of the reactions.

3.2. Activation Strain Model. To gain insight into how anion assistance affects the activation barriers of the different oxidative insertion reactions, i.e., insight into how this effect depends on the nature of the concomitant geometrical deformation and electronic structure of catalyst and substrate, they were analyzed using the Activation Strain model of chemical reactivity.[10,12] In this model, the activation energy $\Delta E^{\ddagger}$ is decomposed into the activation strain $\Delta E^{\ddagger}_{strain}$ and the transition state (TS) interaction $\Delta E^{\ddagger}_{int}$ (see eq 10 and Figure 7):

$$\Delta E^{\ddagger} = \Delta E^{\ddagger}_{strain} + \Delta E^{\ddagger}_{int} \qquad (10)$$

Table 4. Analysis of the Activation Energies for Pd and $PdCl^-$ Induced Activation of the Indicated Bonds of H_2, CH_4, C_2H_6 and CH_3Cl through Direct Oxidative Insertion and, for C−Cl, Also S_N2 Substitution in Terms of the Activation Strain Model

	H_2 (H−H)		CH_4 (C−H)		C_2H_6 (C−H)		C_2H_6 (C−C)		CH_3Cl (C−Cl)		CH_3Cl (C−Cl) via S_N2	
	Pd	$PdCl^-$[a]	Pd	$PdCl^-$	Pd	$PdCl^-$	Pd	$PdCl^-$	Pd	$PdCl^-$	Pd	$PdCl^-$
Energy Decomposition (in kcal/mol)												
$\Delta E^{\ddagger}$	−21.7	−35.3	−1.6	−11.1	−0.7	−10.3	12.6	9.1	−4.3	−10.3	24.5	−18.5
$\Delta E^{\ddagger}_{strain}$	55.6	56.1	53.5	49.7	54.7	58.1	39.4	36.3	8.8	9.6	87.7	91.8
$\Delta E^{\ddagger}_{int}$	−77.3	−91.4	−55.1	−60.8	−55.4	−68.4	−26.8	−27.2	−13.1	−19.9	−63.2	−110.3
ΔE_{Pauli}	208.7	176.3	211.1	169.4	209.8	184.1	192.6	180.7	112.3	89.3	112.5	162.2
ΔV_{elst}	−183.7	−173.6	−170.4	−143.3	−171.9	−159.2	−139.5	−126.1	−76.7	−66.9	−74.2	−117.7
ΔE_{oi}	−102.3	−94.1	−95.8	−86.9	−93.3	−93.3	−79.9	−81.8	−48.7	−42.3	−101.4	−154.7
Fragment Orbital Overlap ⟨Catalyst|Substrate⟩[b]												
⟨HOMO|HOMO⟩	0.256	0.126	0.260	0.153	0.306	0.206	0.158	0.063	0.180[c]	0.117	0.146[d]	0.275[d]
⟨HOMO|LUMO⟩	0.300	0.343	0.327	0.496	0.450	0.539	0.136	0.093	0.082	0.087	0.228	0.403
⟨LUMO|HOMO⟩	0.566	0.709	0.401	0.425	0.359	0.396	0.213	0.212	0.144[c]	0.229	0.174[d]	0.070[d]
Fragment Orbital Population (in Electrons)[b]												
cat. LUMO	0.45	0.21	0.38	0.10	0.38	0.11	0.22	0.04	0.18	0.11	0.22	0.10
cat. HOMO	9.28	9.32	9.32	9.34	9.31	9.27	9.42	9.32	9.59	9.57	9.26	8.97
substr. LUMO	0.43	0.57	0.36	0.46	0.36	0.51	0.25	0.31	0.17	0.31	0.64	0.98
substr. HOMO	1.73	1.89	1.71	1.85	1.74	1.86	1.83	1.89	1.91[c]	1.90	1.78[d]	1.83[d]

[a] No stable product. Analysis based on fictitious TS structure corresponding to the TS structure for Pd + H_2 frozen with Cl^- added and an optimized Pd−Cl distance of 2.370 Å. [b] For Pd, HOMO refers to the five degenerated 4*d* AOs and their combined overlaps or populations. For $PdCl^-$, HOMO refers to the 5σ, two 3π and two 1δ orbitals and their combined overlaps or populations. The Pd LUMO is the 5*s*, the $PdCl^-$ LUMO is the 6σ (see also Scheme 1). [c] Values for substrate HOMO-1 instead of HOMO are given. In the TS for OxIn of Pd into the C−Cl bond of CH_3Cl, the lone pair on Cl in A′ symmetry that overlaps and interacts with the model catalyst's HOMO or LUMO is the HOMO-1 not the HOMO. [d] Values for substrate HOMO-2 instead of HOMO are given. In the TS for S_N2/Cl-ra of Pd or $PdCl^-$ + CH_3Cl, it is the substrate HOMO-2, i.e., the bonding σ_{CCl} (not the HOMO) that overlaps and interacts most strongly with the model catalyst's HOMO or LUMO.

The activation strain $\Delta E^{\ddagger}_{strain}$ is the strain energy associated with deforming the reactants from their equilibrium geometry to the geometry they acquire in the activated complex (Figure 7). The TS interaction $\Delta E^{\ddagger}_{int}$ is the actual interaction energy between the deformed reactants in the transition state. In the present study, one of the reactants is either the neutral, uncoordinated Pd-d^{10} atom or the anionic model complex $PdCl^-$ and the other reactant is one of the substrates H_2, CH_4, C_2H_6, and CH_3Cl.

The TS interaction $\Delta E^{\ddagger}_{int}$ between the strained reactants is further analyzed in the conceptual framework provided by the Kohn−Sham molecular orbital (KS-MO) model.[16] To this end, it is further decomposed into three physically meaningful terms (eq 11) using the extended transition state (ETS) method[22] developed by Ziegler and Rauk.

$$\Delta E^{\ddagger}_{int} = \Delta V_{elst} + \Delta E_{Pauli} + \Delta E_{oi} \qquad (11)$$

The term ΔV_{elst} corresponds to the classical electrostatic interaction between the unperturbed charge distributions of the deformed reactants and is usually attractive. The Pauli repulsion ΔE_{Pauli} comprises the destabilizing interactions between occupied orbitals and is responsible for the steric repulsion. The orbital interaction ΔE_{oi} accounts for charge transfer (interaction between occupied orbitals on one moiety with unoccupied orbitals of the other, including the HOMO−LUMO interactions) and polarization (empty-occupied orbital mixing on one fragment due to the presence of another fragment).

3.3. Analysis of the Reaction Barriers for Bond Activation. The results of the Activation Strain analysis are listed in Table 4. Anion assistance, as mentioned above, lowers the reaction barrier for all bonds and for both types of mechanisms, i.e., direct oxidative insertion (OxIn) and the S_N2 pathway. The effect of anion assistance is major if we consider the competition between the latter two pathways for C−Cl bond activation, which shifts from OxIn (retention of configuration at C in C−Cl) to S_N2 pathway (inversion of configuration). As will become clear below, a quite straightforward and comprehensible physical mechanism hides behind this effect. But first we focus on understanding the somewhat more subtle mechanism of anion assistance in case of direct oxidative insertion into H−H, C−H, C−C and C−Cl bonds. Note that in the case of $PdCl^-$ + H−H, the reverse barrier for oxidative insertion actually disappears and that therefore no stable product or TS exist. To nevertheless allow for a comparison with the situation of the corresponding neutral reaction of Pd + H−H and how this is affected by anion assistance, we have analyzed a fictitious TS for oxidative insertion of $PdCl^-$ + H−H. This fictitious TS has been obtained by using the geometry of corresponding TS **1c** for the insertion of uncoordinated Pd into H_2 and adding a Cl^- ligand to Pd, keeping the PdH_2 portion frozen and only optimizing the Pd−Cl distance of the C_{2v} symmetric species, yielding Pd−Cl = 2.370 Å (see Table 4).

Activation Strain Analysis of OxIn Pathways. The activation energy $\Delta E^{\ddagger}$ varies, not unexpectedly, from one model reaction to another. Interestingly, the activation strain $\Delta E^{\ddagger}_{strain}$ fluctuates much less and, in fact, adopts values that for each type of bond are in a characteristic range (see Table 4). The lowering of the activation barriers through anion assistance is in most cases caused by the TS interaction $\Delta E^{\ddagger}_{int}$ becoming more stabilizing. This is so especially if the effects become relatively large, as for H−H activation, whereas the

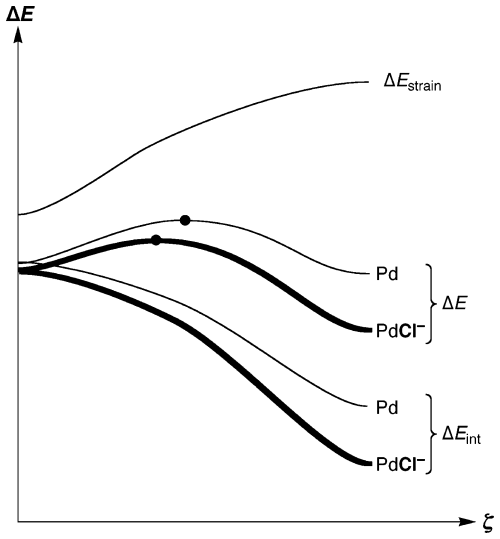

Figure 8. Schematic representation of typical reaction profiles provided by the energy ΔE of the reaction system for direct oxidative insertion of Pd (thin lines) and $PdCl^-$ (bold lines) into an H−H or C−X bond, and its decomposition into the strain energy ΔE_{strain} of and interaction energy ΔE_{int} between substrate and catalyst. Note that anion assistance stabilizes the TS (bullet) and shifts it back along the reaction coordinate ζ (the extent of H−H or C−X bond stretching) toward the reactant side at the left.

situation becomes less clear-cut in case of marginal anion assistance, as for C−C activation. For example, going from Pd to $PdCl^-$, the barrier of the H−H bond activation is reduced from −21.7 kcal/mol to −35.3 kcal/mol (note that the latter value refers to a fictitious TS, vide supra), the activation strain remains in the same order, ca. 56 kcal/mol, and the strength of the TS interaction increases from −77.3 kcal/mol to −91.4 kcal/mol. Overall, for H−H, C−H (in methane and ethane) and C−Cl bond activation, anion assistance lowers barriers by 6−14 kcal/mol, which stems mainly from the strengthening of the TS interaction by 6−13 kcal/mol, whereas the activation strain changes only by 1−4 kcal/mol. Note that in the case of H−H, the energy of what can be conceived as the range of the PES where the TS might occur is stabilized more than the range of the PES where the product might occur. As a result, anion assistance makes the reverse barrier for insertion of $PdCl^-$ into the H−H bond disappear and there is thus no longer a stable product. Anion assistances has hardly any effect on C−C bond activation: both the reduction of the barrier $\Delta E^{\ddagger}$ (by 3.5 kcal/mol) and the changes in its components $\Delta E^{\ddagger}_{strain}$ and $\Delta E^{\ddagger}_{int}$ (3.1 and 0.4 kcal/mol) are marginal compared to the situation for the other bonds.The activation strain appears to be related to the bond strength of the activated bond and with the percentage-wise extent of bond stretching in the transition state. Typical strengths and lengths of the bonds under investigation are as follows: 104 (H−H), 99 (C−H), 83 (C−C) and 78 kcal/mol (C−Cl), and ∼0.7 (H−H), ∼1.1 (C−H), ∼1.5 (C−C) and ∼1.8 Å (C−Cl).[23] Furthermore, we recall that the percentage-wise extent of bond stretching in the TS for oxidative insertion is 85% (H−H), 44−51% (C−H), 24−26% (C−C) and 9−13% (C−Cl, see Table 2). Thus, both the bond strength and the percentage-wise bond elongation in the TS decrease in the order H−H > C−H > C−C > C−Cl. This correlates well with the activation strain, which decreases in approximately the same order, namely, along H−H ≈ C−H (50−58 kcal/mol) > C−C (36−39 kcal/mol) > C−Cl (∼9 kcal/mol, see Table 4).[24]

Note that anion assistance causes reduction in activation strain (Table 4) and a contraction of the activated bond in the TS (Table 2) in case of methane C−H and ethane C−C bond activation. One might at first expect the opposite, namely, that the stronger catalyst-substrate interaction in case of $PdCl^-$ causes the palladium atom to be further inserted into the activated bond in the TS. An understanding of these (and other) more subtle variations in activation strain $\Delta E^{\ddagger}_{strain}$ requires that we take into account that the precise location of the TS (and thus the values of $\Delta E^{\ddagger}_{strain}$ and $\Delta E^{\ddagger}_{int}$) is the result of achieving, along the reaction coordinate ζ, a (labile) balance between reactants strain $\Delta E_{strain}(\zeta)$ and catalyst-substrate interaction $\Delta E_{int}(\zeta)$. While such detailed analyses are beyond the scope of the present work, we wish to report here preliminary results that provide a simple way of understanding the above-mentioned reduction in $\Delta E^{\ddagger}_{strain}$ and contraction of activated bonds in the TS, caused by anion assistance. Figure 8 shows a schematic representation of a typical reaction profile. First, we examine the energy profile (ΔE) for the Pd-induced reaction, which is decomposed into the strain energy $\Delta E_{strain}(\zeta)$ of the reactants plus their mutual interaction energy $\Delta E_{int}(\zeta)$. Along the reaction coordinate ζ, $\Delta E_{strain}(\zeta)$ increases because the C−X bond of the substrate is stretched, while the Pd-substrate interaction $\Delta E_{int}(\zeta)$ becomes more stabilizing due to the decreasing HOMO−LUMO gap of the deformed substrate. The net result is the reaction profile of ΔE with the transition state indicated by a bullet (thin lines in Figure 8). Note that the reaction coordinate can be represented as the extent of stretching of the H−H or C−X bond. Next, we switch on anion assistance. This has not much effect on the $\Delta E_{strain}(\zeta)$ curve, which closely resembles the C−X bond dissociation profile in both the Pd and $PdCl^-$ induced reactions. The catalyst-substrate interaction, on the other hand, is substantially stabilized due to anion assistance and this strengthening becomes larger as the reaction proceeds (see bold lines in Figure 8). This is so simply because the inherent strength of the Pd-substrate interaction also increases along this direction (vide supra). Thus, the $\Delta E_{int}(\zeta)$ curve is stabilized and it becomes steeper. Therefore, also the energy (ΔE) profile and, thus, all stationary points of the $PdCl^-$ induced reaction are stabilized and, because of the steeper descent of $\Delta E_{int}(\zeta)$, the maximum shifts to the left, i.e., the TS becomes more reactant-like. This implies that the activated bond is less stretched and the activation strain somewhat reduced, compared to the corresponding Pd-induced reaction. Note that the observed behavior, i.e., the shift of the TS geometry toward the educt side in case of a more exothermic reaction, is reminiscent of the Hammond postulate[25] and that the origin and working of this postulate emerges naturally in terms of the Activation strain model as being the result of the interplay between the strain $\Delta E_{strain}(\zeta)$, which remains constant, and interaction $\Delta E_{int}(\zeta)$, which increases here as we go from Pd to $PdCl^-$. We plan to extend this type of analyses also to the ethane

C−H and the C−Cl bond which show another, yet unexplained behavior.

Whereas the activation strain $\Delta E^{\ddagger}_{\text{strain}}$ appears to correlate well with the strength and length of the activated bond,[24] there is no such straightforward relationship at all for the activation barrier $\Delta E^{\ddagger}$ which shows a more complex behavior. This is so, of course, because $\Delta E^{\ddagger}$ arises as the sum of $\Delta E^{\ddagger}_{\text{strain}}$ *and* $\Delta E^{\ddagger}_{\text{int}}$, and it mirrors the interplay of the trends, often mutually counteracting, in *both* of these two quantities. The TS interaction $\Delta E^{\ddagger}_{\text{int}}$ becomes less stabilizing in the order H−H > C−H > C−C > C−Cl. We have shown previously[12a] for the Pd-induced reactions and find here again for the $PdCl^-$-induced reactions that this trend is to an important extent determined by the donor−acceptor orbital interactions between occupied Pd 4*d* AOs and the empty $\sigma^*_{\text{C–X}}$ (or $\sigma^*_{\text{H–H}}$) acceptor orbital associated with the bond to be activated in the substrate (see Table 4). The orbital interactions decrease along H−H, C−H and C−C because the σ^* acceptor orbital of the substrate in the TS goes up in energy leading to a larger HOMO−LUMO gap with the Pd 4*d* AOs. They further decrease from C−C to C−Cl because of a relatively small Pd 4*d*−CH_3Cl $\sigma^*_{\text{C–Cl}}$ overlap. This trend is reinforced by the electrostatic attraction ΔV_{elst}, which also decreases along H−H, C−H, C−C and C−Cl as the Pd-substrate distance increases along this series (see Table 4 and Figures 1−5), and by the donor−acceptor orbital interactions between substrate HOMO and catalyst LUMO, which is however less important, in particular for the negatively charged and thus poorly electron-accepting $PdCl^-$ (see, e.g., the much smaller population of the $PdCl^-$ versus the Pd LUMO in Table 4).

Here, we address the question *why* anion assistance leads to an increased, more stabilizing TS interaction $\Delta E^{\ddagger}_{\text{int}}$. Our Kohn−Sham orbital analyses show that the bonding frontier-orbital interactions are provided by the following: (i) back-donation from the occupied metal 4*d* (or metal−ligand 4*d* hybrid) orbitals to the unoccupied C−X (or H−H) σ^* antibonding orbital of the substrate and (ii) donation from the occupied C−X (or H−H) σ bonding orbital of the substrate to the unoccupied metal 5*s* (or metal−ligand 5*s* hybrid) orbital (see also ref 12a). In addition, there is an important Pauli-repulsive (i.e., occupied-occupied) interaction between the metal 4*d* (or metal−ligand 4*d* hybrid) orbitals and the C−X (or H−H) σ bonding orbital. In the case of C−Cl, the most important occupied-occupied repulsion is that with the lone-pair on chlorine pointing toward the metal; this lone-pair orbital is the HOMO of chloromethane (see also ref 12a). The effect of anion assistance can now be understood in terms of how these bonding and repulsive orbital interactions are affected as the Cl^- ligand coordinates to the metal. The main effect of this coordination is that the palladium 4*d* orbitals are pushed up in energy and split into $4d_\pi$, $4d_\sigma$ and $4d_\delta$ (this splitting is however marginal, i.e., ca. 0.1 eV), as shown in Scheme 1.

Also the shape of the 4*d* AOs changes: they are Pd−Cl antibonding combinations with a small bonding admixture of Pd 5*p*; this is illustrated in Scheme 1 for the Pd $4d_{xz}$ and $PdCl^-$ "$4d_\pi$" orbitals. These changes in the catalyst's electronic structure reduce the metal "4*d*"-substrate σ^* orbital-energy gap, whereas they increase the substrate σ (or Cl lone pair)-metal "5*s*" orbital energy gap (as illustrated in Scheme 2), which causes two counteracting effects: back-donation is reinforced and donation is weakened.

Scheme 1. Cl− Ligand Pushes up and Splits Pd 4*d* Orbitals

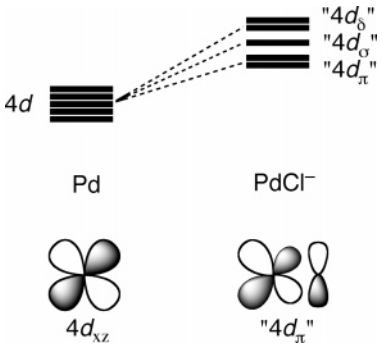

Scheme 2. Frontier Orbitals of Pd, PdCl− and H_3C-X

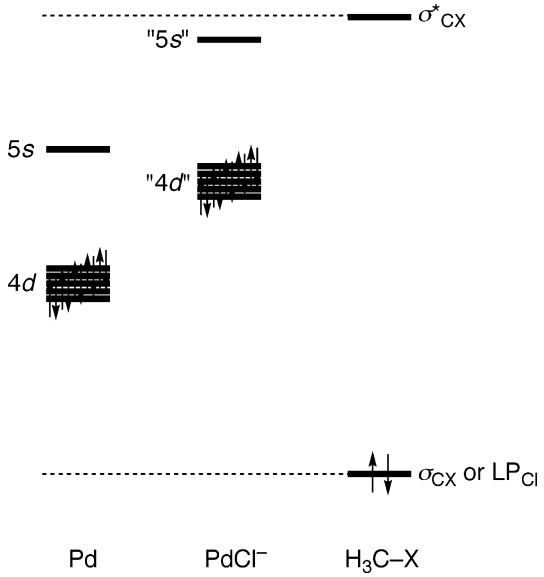

Thus, overall, only moderate changes in the bonding orbital interactions are expected. The Pauli repulsive orbital interactions, on the other hand, are expected to become less repulsive in the case of anion assistance as the HOMO−HOMO energy gap between metal "4*d*" and substrate σ (or, for CH_3Cl, LP_{Cl}) increases and, as shown in Table 4, the corresponding overlap decreases. The quantitative decomposition of the TS interactions $\Delta E^{\ddagger}_{\text{int}}$ indeed confirms these qualitative expectations (see Table 4). It shows that the increased stabilization of $\Delta E^{\ddagger}_{\text{int}}$ in the case of $PdCl^-$ stems primarily from a reduction in Pauli repulsion ΔE_{Pauli} (by −12 to −42 kcal/mol), whereas the bonding orbital interactions ΔE_{oi} change much less (by −2 to 9 kcal/mol) and the electrostatic attraction ΔV_{elst} becomes somewhat less stabilizing (by 10 to 27 kcal/mol).

OxIn versus S_N2 Pathways to C−X Bond Activation. Finally, we aim at a simple, physical understanding of *why* anion assistance causes a switch of mechanistic pathway for C−Cl bond activation from direct oxidative insertion (barriers for Pd: −6.0 kcal/mol for OxIn versus 21.2 kcal/mol for S_N2) to S_N2 substitution (barriers for $PdCl^-$: −11.2 kcal/

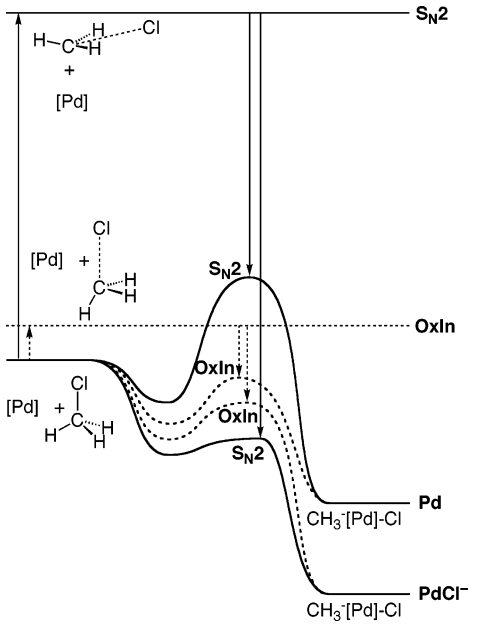

Figure 9. Fragment-oriented Design of a Catalyst (FDC) for stereoselective C−Cl bond activation based on the Activation Strain model: reaction profiles and Activation Strain analyses ($\Delta E^{\ddagger}_{strain}$: arrows up, $\Delta E^{\ddagger}_{int}$: arrows down) for oxidative addition of Pd or $PdCl^-$ to the H_3C-Cl bond through oxidative insertion (OxIn, dashed lines) and S_N2 substitution pathways (straight lines).

mol for OxIn versus −20.2 kcal/mol for S_N2) and, thus, from retention of configuration at the carbon atom to inversion of this configuration (see Table 1 and Section 3.1). Again, it appears from the activation strain analysis that the activation strain $\Delta E^{\ddagger}_{strain}$ is relatively constant and, thus, a characteristic for a particular mechanism: it is low (8.8 kcal/mol for Pd and 9.6 kcal/mol for $PdCl^-$; see Table 4) for the OxIn pathway in which the C−Cl bond is only slightly elongated, and it is high (87.7 kcal/mol for Pd and 91.8 kcal/mol for $PdCl^-$; see Table 4) for the S_N2 pathway in which chloromethane must undergo a major deformation as the Cl^- leaving group migrates around CH_3 toward the palladium atom. It is the TS interaction $\Delta E^{\ddagger}_{int}$ that is responsible for both the fact that the barriers for both pathways decrease through anion assistance and the fact that this decrease is much stronger for the S_N2 pathway which, therefore, becomes the preferred mechanism. This is illustrated in Figure 9, which shows the potential energy surfaces (PES) of the OxIn and S_N2 pathways for C−Cl activation by Pd and $PdCl^-$.[21]

Now, a simple picture emerges of how anion assistance works and how we can rationally design a catalyst's selectivity for, in this example, the stereochemical course of C−X bond activation. The two pathways for this process are associated with very different geometrical reorganizations of the substrate and, thus, pronouncedly different and characteristic values for the activation strain: the latter is high for the S_N2 pathway and low for direct insertion. The strong distortions that are responsible for the high activation strain for S_N2 also cause the TS interaction for this pathway to be more stabilizing than for OxIn. This is because going from the overall transition state for OxIn to that for the S_N2 pathway, the C−Cl antibonding σ^* acceptor orbital drops by ca. 4.6 eV in energy (not shown in Table 4) as the C−Cl bond is more elongated and, thus, becomes a better partner in the HOMO−LUMO interaction with the HOMO of a given catalyst. If this catalyst is one that interacts relatively weakly with the substrate, such as the uncoordinated Pd atom, the TS interaction cannot reverse the trend in activation strains and, as a result, direct oxidative insertion (OxIn) with its low activation strain remains the preferred mechanism, leading to C*−Cl bond activation with retention of configuration at C*. However, if we make the catalyst a sufficiently good electron donor, e.g., by pushing up the energy of the 4*d* orbitals with a Cl^- ligand, as in our model catalyst $PdCl^-$, the TS interaction can become strong enough to take over the role of trend setter, that is, to *reverse* the trend and make S_N2 substitution, despite its high activation strain, the dominant pathway, leading to C*−Cl bond activation with inversion of configuration at C*.

4. Conclusions

Anion assistance, i.e., coordination of a Cl^- ligand to the metal atom, lowers the activation barriers of the Pd(0)-catalyzed activation of prototypical C−H, C−C and C−Cl bonds. Activation enthalpies $\Delta H^{\ddagger}_{298}$ for oxidative insertion (OxIn) of $PdCl^-$ into the various types of bonds (computed at ZORA-BP86/TZ(2)P) are lower than the corresponding ones for Pd, but they increase essentially in the same order, namely, along C−H ≈ C−Cl < C−C.

The effect of anion assistance is selective: it favors the highly endothermic S_N2 mechanism over direct oxidative insertion (OxIn). Interestingly, in the case of C*−Cl bond activation in CH_3Cl, this leads to a shift in mechanism and stereochemistry, namely, from the OxIn pathway that goes with retention of configuration at C* to the S_N2 pathway that goes with inversion of configuration at C*. This is of practical relevance for substrates in which C* is asymmetric (which is obviously not the case in our simple model system).

To obtain a physical understanding of how anion assistance works, we have analyzed the various model reactions using the Activation Strain model in which the activation energy $\Delta E^{\ddagger}$ is decomposed into the activation strain $\Delta E^{\ddagger}_{strain}$ of and the stabilizing transition state (TS) interaction $\Delta E^{\ddagger}_{int}$ between the reactants in the activated complex: $\Delta E^{\ddagger} = \Delta E^{\ddagger}_{strain} + \Delta E^{\ddagger}_{int}$. Interestingly, the activation strain $\Delta E^{\ddagger}_{strain}$ adopts characteristic values for a particular type of bond and reaction mechanism, e.g., low for C−Cl activation through OxIn and high for C−Cl activation through S_N2. The lowering of activation barriers upon anion assistance is primarily caused by a stronger, more stabilizing TS interaction $\Delta E^{\ddagger}_{int}$. This increase in $\Delta E^{\ddagger}_{int}$ can be ascribed to the raise in Pd-4*d* derived orbitals in $PdCl^-$ which translates, among others, into more stabilizing donor−acceptor orbital interactions between the metal and the substrate.

The case of C−Cl bond activation exemplifies how a catalyst's selectivity regarding retention or inversion of configuration of the carbon atom in the activated bond can be tuned by simply increasing or decreasing the TS interaction. Eventually, we wish to apply this approach to rationally tuning, through a clever choice of ligands, a

catalyst's selectivity for a particular bond in a substrate, e.g., C−H versus C−C.

Acknowledgment. We thank the Fonds der Chemischen Industrie (FCI) for a doctoral stipendium for A.D. and The Netherlands Organization for Scientific Research (NWO-CW) for financial support.

References

(1) (a) Collman, J. P.; Hegedus, L. S.; Norton, J. R.; Finke, R. G. *Principles and Applications of Organotransition Metal Chemistry*; University Science Books: Mill Valley, CA, 1987. (b) Elschenbroich, Ch.; Salzer, A. *Organometallics. A Concise Introduction*, 2nd ed.; VCH: Weinheim, Germany, 1992. (c) Amatore, C.; Jutand, A. *Acc. Chem. Res.* **2000**, *33*, 314. (d) Yang, H.; Kotz, K. T.; Asplund, M. C.; Wilkens, M. J.; Harris, C. B. *Acc. Chem. Res.* **1999**, *32*, 551.

(2) Experimental studies on reactions of metal complexes in the condensed phase: (a) Luh, T.-Y.; Leung, M.-k.; Wong, K.-T. *Chem. Rev.* **2000**, *100*, 3187. (b) Stürmer, R. *Angew. Chem.* **1999**, *111*, 3509. (c) Hau, L.-B.; Tanaka, M. *Chem. Commun.* **1999**, *5*, 395. (d) Casado, A. L.; Espinet, P. *Organometallics* **1998**, *17*, 954. (e) Kayser, B.; Missling, C.; Knizek, J.; Noeth, H.; Beck, W. *Eur. J. Inorg. Chem.* **1998**, *3*, 375. (f) Guillevic, M.-A.; Rocaboy, C.; Arif, A. M.; Horvath, I. T.; Gladysz, J. A. *Organometallics* **1998**, *17*, 707. (g) Edelbach, B. L.; Lachicotte, R. J.; Jones, W. D. *J. Am. Chem. Soc.* **1998**, *120*, 2843. (h) Crabtree, R. H. *Chem. Rev.* **1995**, *95*, 987. (i) Grushin, V. V.; Alper, H. *Chem. Rev.* **1994**, *94*, 1047. (j) Ellis, P. R.; Pearson, J. M.; Haynes, A.; Adams, H.; Bailey, N. A.; Maitlis, P. M. *Organometallics* **1994**, *13*, 3215. (k) Wright, M. W.; Smalley, T. L.; Welker, M. E.; Rheingold, A. L. *J. Am. Chem. Soc.* **1994**, *116*, 6777. (l) Sakakaurka, T.; Sodeyama, T.; Sasaki, K.; Wada, K.; Tanaka, M. *J. Am. Chem. Soc.* **1990**, *112*, 7221. (m) Casalnuovo, A. L.; Calabrese, J. C.; Milstein, D. *J. Am. Chem. Soc.* **1988**, *110*, 6738. (n) Janowics, A. H.; Bergman, R. G. *J. Am. Chem. Soc.* **1983**, *105*, 3929. (o) Jones, W. D.; Feher, F. J. *J. Am. Chem. Soc.* **1982**, *104*, 4240.

(3) (a) Hickey, C. E.; Maitlis, P. M. *J. Chem. Soc., Chem. Commun.* **1984**, 1609. (b) Forster, D. *Adv. Organomet. Chem.* **1979**, *17*, 255. (c) Forster, D. *J. Am. Chem. Soc.* **1975**, *97*, 951.

(4) Experimental studies on reactions of ionic metal atoms and complexes in the gas phase: (a) Brönstrup, M.; Schröder, D.; Schwarz, H. *Organometallics* **1999**, *18*, 1939. (b) Aschi, M.; Brönstrup, M.; Diefenbach, M.; Harvey, J. N.; Schröder, D.; Schwarz, H. *Angew. Chem.* **1998**, *110*, 858. (c) Freiser, B. S. *J. Mass Spectrom.* **1996**, *31*, 703. (d) van Koppen, P. A. M.; Kemper, P. R.; Bushnell, J. E.; Bowers, M. T. *J. Am. Chem. Soc.* **1995**, *117*, 2098. (e) Wesendrup, R.; Schröder, D.; Schwarz, H. *Angew. Chem.* **1994**, *105*, 1232. (f) Chen, Y.-M.; Clemmer, D. E.; Armentrout, P. B. *J. Am. Chem. Soc.* **1994**, *116*, 7815. (g) van den Berg, K. J.; Ingemann, S.; Nibbering, N. M. M.; Gregor, I. K. *Rapid. Commun. Mass Spectrom.* **1993**, *7*, 769. (h) Chowdhury, A. K.; Wilkins, C. L. *J. Am. Chem. Soc.* **1987**, *109*, 5336. (i) Weil, D. A.; Wilkins, C. L. *J. Am. Chem. Soc.* **1985**, *107*, 7316. (j) Jones, R. W.; Staley, R. H. *J. Phys. Chem.* **1982**, *86*, 1669. (k) Jones, R. W.; Staley, R. H. *J. Am. Chem. Soc.* **1980**, *102*, 3794.

(5) Combined experimental and theoretical studies on reactions of ionic metal atoms and complexes in the gas phase: (a) Yi, S. S.; Reichert, E. L.; Holthausen, M. C.; Koch, W.; Weisshaar, J. C. *Chem. Eur. J.* **2000**, *6*, 2232. (b) Blomberg, M.; Yi, S. S.; Noll, R. J.; Weisshaar, J. C. *J. Phys. Chem. A* **1999**, *103*, 7254. (c) Diefenbach, M.; Brönstrup, M.; Aschi, M.; Schröder, D.; Schwarz, H. *J. Am. Chem. Soc.* **1999**, *121*, 10614. (d) Schwarz, J.; Schröder, D.; Schwarz, H.; Heinemann, C.; Hrusák, J. *Helv. Chim. Acta* **1996**, *79*, 1110.

(6) Experimental studies on reactions of neutral metal atoms in the gas phase: (a) Wen Y.; Porembski, M.; Ferrett, T. A.; Weisshaar, J. C. *J. Phys. Chem. A* **1998**, *102*, 8362. (b) Wen, Y.; Yethiraj, A.; Weisshaar, J. C. *J. Chem. Phys.* **1997**, *106*, 5509. (c) Carroll, J. J.; Weisshaar, J. C. *J. Phys. Chem.* **1996**, *100*, 12355. (d) Chertihin, G. V.; Andrews, L. *J. Am. Chem. Soc.* **1994**, *116*, 8322. (e) Carroll, J. J.; Haug, K. L.; Weisshaar, J. C. *J. Am. Chem. Soc.* **1993**, *115*, 6962. (f) Carroll, J. J.; Weisshaar, J. C. *J. Am. Chem. Soc.* **1993**, *115*, 800. (g) Ritter, D.; Carroll, J. J.; Weisshaar, J. C. *J. Phys. Chem.* **1992**, *96*, *10636*. (h) Mitchell, S. A.; Hackett, P. A. *J. Chem. Phys.* **1990**, *93*, 7822. (i) Ritter, D.; Weisshaar, J. C. *J. Am. Chem. Soc.* **1990**, *112*, 6425. (j) Fayet, P.; Kaldor, A.; Cox, D. M. *J. Chem. Phys.* **1990**, *92*, 254.

(7) Combined experimental and theoretical studies on reactions of neutral metal atoms in the gas phase: (a) Porembski, M.; Weisshaar, J. C. *J. Phys. Chem. A* **2000**, 104, 1524. (b) Carroll, J. J.; Haug, K. L.; Weisshaar, J. C.; Blomberg, M. R. A.; Siegbahn, P. E. M.; Svensson, M. *J. Phys. Chem.* **1995**, *99*, 13955. (c) Carroll, J. J.; Weisshaar, J. C.; Siegbahn, P. E. M.; Wittborn, A. M. C.; Blomberg, M. R. A. *J. Phys. Chem.* **1995**, *99*, 14388. (d) Mitchell, S.; Blitz, M. A.; Siegbahn, P. E. M.; Svenson, M. *J. Chem. Phys.* **1994**, *100*, 423. (e) Weisshaar, J. C. *Acc. Chem. Res.* **1993**, *26*, 213.

(8) Theoretical studies on reactions of metal complexes: (a) Dedieu, A. *Chem. Rev.* **2000**, *100*, 543. (b) Torrent, M.; Solà, M.; Frenking, G. *Chem. Rev.* **2000**, *100*, 439. (c) Griffin, T. R.; Cook, D. B.; Haynes, A.; Pearson, J. M.; Monti, D.; Morris, G. E. *J. Am. Chem. Soc.* **1996**, *118*, 3029. (d) Aullón, G.; Alvarez, S. *Inorg. Chem.* **1996**, *35*, 3137. (e) Ziegler, T. *Chem. Rev.* **1991**, *91*, 651. (f) Koga, N.; Morokuma, K. *Chem. Rev.* **1991**, *91*, 823. (g) Bickelhaupt, F. M.; Baerends, E. J.; Ravenek, W. *Inorg. Chem.* **1990**, *29*, 350.

(9) Bickelhaupt, F. M.; Ziegler, T.; von Ragué Schleyer, P. *Organometallics* **1995**, *14*, 2288.

(10) Bickelhaupt, F. M. *J. Comput. Chem.* **1999**, *20*, 114.

(11) Theoretical studies on reactions of neutral metal atoms: (a) Maseras, F.; Lledós, A.; Clot, E.; Eisenstein, O. *Chem. Rev.* **2000**, *100*, 601. (b) Cui, Q.; Musaev, D. G.; Morokuma, K. *J. Chem. Phys.* **1998**, *108*, 8418. (c) Wittborn, A. M. C.; Costas, M.; Blomberg, M. R. A.; Siegbahn, P. E. M. *J. Chem. Phys.* **1997**, *107*, 4318. (d) Siegbahn, P. E. M. *J. Am. Chem. Soc.* **1994**, *116*, 7722. (e) Siegbahn, P. E. M. *Organometallics* **1994**, *13*, 2833. (f) Perry, J. K.; Ohanessian, G.; Goddard, W. A., III *Organometallics* **1994**, *13*, 1870. (g) Blomberg, M. R. A.; Siegbahn, P. E. M.; Svensson, M. *Inorg. Chem.* **1993**, *32*, 4218. (h) Siegbahn, P. E. M.; Blomberg, M. R. A.; Svensson, M. *J. Phys. Chem.* **1993**, *97*, 2564. (i) Siegbahn, P. E. M.; Blomberg, M. R. A.; Svensson, M. *J. Am. Chem. Soc.* **1993**, *115*, 1952. (j) Siegbahn, P. E. M.; Blomberg, M. R. A.; Svensson, M. *J. Am. Chem. Soc.* **1993**, *115*, 4191. (k) Siegbahn, P. E. M.; Blomberg, M. R. A. *J. Am. Chem. Soc.* **1992**, *114*, 10548. (l) Blomberg, M. R. A.; Siegbahn, P. E. M.; Svensson, M. *J. Am. Chem. Soc.* **1992**, *114*, 6095. (m) Svensson, M.; Blomberg, M. R. A.; Siegbahn, P. E. M. *J. Am. Chem. Soc.* **1991**, *113*, 3, 7076. (n) Novaro, O.; Jarque, C. *Theor. Chim. Acta* **1991**, *80*, 19. (o) Blomberg, M. R. A.; Siegbahn, P. E. M.; Nagashima, U.; Wennerberg, J. *J. Am. Chem. Soc.* **1991**, *113*, 424. (p) Carter, E. A.;

Goddard, W. A., III *J. Phys. Chem.* **1988**, *92*, 5679. (q) Nakatsuji, H.; Hada, M.; Yonezawa, T. *J. Am. Chem. Soc.* **1987**, *109*, 1902. (r) Low, J. J.; Goddard, W. A., III *Organometallics* **1986**, *5*, 609. (s) Koga, N.; Obara, S.; Kitaura, K.; Morokuma, K. *J. Am. Chem. Soc.* **1985**, *107*, 7109. (t) Low, J. J.; Goddard, W. A., III *J. Am. Chem. Soc.* **1984**, *106*, 8321.

(12) (a) Diefenbach, A.; Bickelhaupt, F. M. *J. Phys. Chem. A* **2004**, *108*, 8460. (b) Diefenbach, A.; de Jong, G. Th.; Bickelhaupt, F. M. *Mol. Phys.* **2005**, *103*, in press.

(13) (a) Basile, A.; Fasson, S.; Vitulli, G.; Drioli, E. *Stud. Surf. Sci. Catal.* **1998**, *119*, 453. (b) Malleron, J.-L.; Fiaud, J.-C.; Legros, J.-Y. *Handbook of Palladium Catalyzed Organic Reactions*; Academic Press: 1997. (c) Cornils, R.; Herrmann, W. A. *Applied Homogeneous Catalysis with Organometallic Compounds. Vol. 1;* VCH: Weinheim, 1996; p 394.

(14) Diefenbach, A.; Bickelhaupt, F. M. *J. Chem. Phys.* **2001**, *115*, 4030.

(15) Density functional theory (DFT): (a) Dreizler, R. M.; Gross, E. K. U. *Density Functional Theory. An approach to the Quantum Many-Body Problem*; Springer: Berlin, 1990. (b) Parr, R. G.; Yang, W. *Density-Functional Theory of Atoms and Molecules*; Oxford University Press: New York, 1989.

(16) Kohn−Sham MO model in DFT: (a) Bickelhaupt, F. M.; Baerends, E. J. In *Reviews in Computational Chemistry*, Lipkowitz, K. B., Boyd., D. B., Eds.; Wiley-VCH: New York, 2000; Vol. 15, Chapter 1. (b) Baerends, E. J.; Gritsenko, O. V. *J. Phys. Chem. A* **1997**, *101*, 5383.

(17) Amsterdam Density Functional (ADF) program: (a) te Velde, G.; Bickelhaupt, F. M.; Baerends, E. J.; van Gisbergen, S. J. A.; Fonseca Guerra, C.; Snijders, J. G.; Ziegler, T. *J. Comput. Chem.* **2001**, *22*, 931. (b) Baerends, E. J.; Ellis, D. E.; Ros, P. *Chem. Phys.* **1973**, *2*, 41. (c) Baerends, E. J.; Ros, P. *Chem. Phys.* **1975**, *8*, 412. (d) Baerends, E. J.; Ros, P. *Int. J. Quantum Chem., Quantum Chem. Symp.* **1978**, *S12*, 169. (e) Fonseca Guerra, C.; Snijders, J. G.; te Velde, G.; Baerends, E. J. *Theor. Chem. Acc.* **1998**, *99*, 391. (f) Boerrigter, P. M.; te Velde, G.; Baerends, E. J. *Int. J. Quantum Chem.* **1988**, *33*, 87. (g) te Velde, G.; Baerends, E. J. *J. Comput. Phys.* **1992**, *99*, 84. (h) Snijders, J. G.; Baerends, E. J.; Vernooijs, P. *At. Nucl. Data Tables* **1982**, *26*, 483. (i) Krijn, J.; Baerends, E. J. *Fit-Functions in the HFS-Method; Internal Report* (in Dutch); Vrije Universiteit: Amsterdam, 1984. (j) Slater, J. C. *Quantum Theory of Molecules and Solids Vol. 4*; McGraw-Hill: New York, 1974. (k) Becke, A. D. *J. Chem. Phys.* **1986**, *84*, 4524. (l) Becke, A. *Phys. Rev. A* **1988**, *38*, 3098. (m) Vosko, S. H.; Wilk, L.; Nusair, M. *Can. J. Phys.* **1980**, *58*, 1200. (n) Perdew, J. P. *Phys. Rev. B* **1986**, *33*, 8822 (Erratum: *Phys. Rev. B* **1986**, *34*, 7406). (o) Fan, L.; Ziegler, T. *J. Chem. Phys.* **1991**, *94*, 6057. (p) Versluis, L.; Ziegler, T. *J. Chem. Phys.* **1988**, *88*, 322. (q) Fan, L.; Ziegler, T. *J. Chem. Phys.* **1990**, *92*, 3645. (r) Fan, L.; Versluis, L.; Ziegler, T.; Baerends, E. J.; Ravenek, W. *Int. J. Quantum. Chem., Quantum. Chem. Symp.* **1988**, *S22*, 173.

(18) ZORA approach: (a) Chang, C.; Pelissier, M.; Durand, P. *Phys. Scr.* **1986**, *34*, 394. (b) van Lenthe, E.; Baerends, E. J.; Snijders, J. G. *J. Chem. Phys.* **1993**, *99*, 4597. (c) van Lenthe, E.; Baerends, E. J.; Snijders, J. G. *J. Chem. Phys.* **1994**, *101*, 9783. (d) van Lenthe, E.; van Leeuwen, R.; Baerends, E. J.; Snijders, J. G. *Int. J. Quantum Chem.* **1996**, *57*, 281.

(19) Atkins, P. W. Physical *Chemistry*; Oxford University Press: Oxford, 1998.

(20) A negative activation energy does not imply the complete absence of any barrier. The reaction is still hampered by a statistical or entropic bottleneck that is associated with the decrease in the number of available quantum states (e.g., of translation, rotation, and vibration) as one goes from the separate, unbound reactants to the tightly bound transition state.

(21) Note that the [Pd]-CH_3^+···Cl^- structure, which occurs between the stages of S_N2 substitution and Cl-rearrangement, is labile (i.e., a shoulder on the PES instead of a local minimum) for [Pd] = Pd, while it becomes stable (i.e., a local minimum) in case of [Pd] = $PdCl^-$ (see Table 1 for computed energies). One way of viewing this is that the [Pd]-CH_3^+···Cl^- structure benefits relatively more, in terms of relative stability, from anion assistance than the transition-state structures corresponding to the S_N2 and Cl-rearrangement stages of the mechanism. An alternative but equivalent view is that $PdCl^-$ (with its high-energy HOMO) is a strong enough nucleophile for preventing its spontaneous expulsion by Cl^- while Pd (with its low-energy HOMO) is not.

(22) Bond energy decomposition: (a) Ziegler, T.; Rauk, A. *Inorg. Chem.* **1979**, *18*, 1558. (b) Ziegler, T.; Rauk, A. *Inorg. Chem.* **1979**, *18*, 1755. (c) Ziegler, T.; Rauk, A. *Inorg. Chem.* **1977**, *16*, 1. (d) Bickelhaupt, F. M.; Nibbering, N. M. M.; van Wezenbeek, E. M.; Baerends, E. J. *J. Phys. Chem.* **1992**, *96*, 4864.

(23) Holleman, A. F.; Wiberg, N. *Lehrbuch der Anorganischen Chemie*; de Gruyter: Berlin, 1985.

(24) The present model catalysts contribute only marginal ($PdCl^-$) or not at all (Pd) to the activation strain. We anticipate that introducing more than one ligand into the catalytically active transition metal system brings into play the phenomenon of ligand reorganization as an additional important factor that affects the activation strain of the reaction.

(25) Hammond, G. S. *J. Am. Chem. Soc.* **1955**, *77*, 334.

CT0499478